

# Constraints on the curvature of nuclear symmetry energy from recent astronomical data within the KIDS framework

Hana Gil,<sup>1,\*</sup> Panagiota Papakonstantinou,<sup>2,†</sup> and Chang Ho Hyun<sup>3,‡</sup>

<sup>1</sup>*Center of Extreme Nuclear Matter,*

*Korea University, Seoul 02841, Korea*

<sup>2</sup>*Rare Isotope Science Project, Institute for Basic Science, Daejeon 34047, Korea*

<sup>3</sup>*Department of Physics Education, Daegu University, Gyeongsan 38453, Korea*

(Dated: October 20, 2021)

## Abstract

We investigate the density dependence of the nuclear symmetry energy  $S(\rho)$  in the KIDS (Korea-IBS-Daegu-SKKU) framework for the nuclear equation of state (EoS) and energy-density functional (EDF). The aim is to constrain the value of the curvature parameter ( $K_{\text{sym}}$ ) based on recent astronomical data. First, assuming a standard saturation point, we calculate bulk nuclear properties within KIDS-EDF for different values of the compression modulus of symmetric nuclear matter ( $K_0$ ) and of the leading-order symmetry energy parameters, i.e., the symmetry energy ( $J$ ) and slope ( $L$ ) at saturation density, each within a broadly accepted range, as well as  $K_{\text{sym}}$ . All of the above EoS parameters are varied independently of each other. The skewness parameter ( $Q_{\text{sym}}$ ) is presently kept fixed at 650 MeV. For all EoS parameter sets which describe the selected nuclear data within better than 0.3%, we calculate the neutron-star equation of state and mass-radius relation and analyze the results in terms of Pearson correlation coefficients  $r$ . We find that the value of  $K_{\text{sym}}$  is strongly correlated with the radius of both a canonical and a massive star ( $|r| > 0.9$ ). If we impose that all known astronomical constraints on the neutron star radii must be satisfied, we deduce  $-150 < K_{\text{sym}} < 0$ . As a result, the symmetry energy as a function of the density is consistently found to have an inflection point at  $\rho_0 < \rho < 2\rho_0$ . We take the opportunity to report that the neutron skin thickness of  $^{208}\text{Pb}$  shows no correlation at all with the neutron star radii ( $|r| < 0.1$ ), in contrast with studies which focus on the role of  $L$  only.

---

\*Electronic address: khn1219@gmail.com

†Electronic address: ppapakon@ibs.re.kr

‡Electronic address: hch@daegu.ac.kr

## I. INTRODUCTION

The physics of dense nuclear matter has entered a golden age thanks to previously unattainable data from diverse objects and phenomena in the Universe. They include millisecond pulsars [1, 2], X-ray bursts from low-mass X-ray binaries (LMXBs) [3, 4], compact binaries [5], gravitational waves (GWs) from neutron star merges [6–9], and soft X-rays from pulsars [10, 11]. Most notable regarding the physics of neutron stars may be the possibility to determine the mass and radius of a single object, thus obtaining strong constraints to the mass and radius of neutron stars, and eventually the nuclear equation of state (EoS).

One key issue for dense nuclear matter is to constrain the EoS and in particular the nuclear symmetry energy  $S(\rho)$  at baryonic densities  $\rho$  higher than the saturation density  $\rho_0$  of symmetric nuclear matter [12–15]. By convention, the density dependence is encoded in the values of its derivatives at saturation density. The following expressions for the energy per particle  $\mathcal{E}(\rho, \delta)$  at density  $\rho$  and isospin asymmetry  $\delta$  summarize the necessary definitions:

$$\mathcal{E}(\rho, \delta) = E(\rho) + S(\rho)\delta^2 + O(\delta^4), \quad (1)$$

$$E(\rho) = E_0 + \frac{1}{2}K_0x^2 + \frac{1}{6}Q_0x^3 + \dots, \quad (2)$$

$$S(\rho) = J + Lx + \frac{1}{2}K_{\text{sym}}x^2 + \frac{1}{6}Q_{\text{sym}}x^3 + \dots. \quad (3)$$

Denoting the neutron and proton densities as  $\rho_n$  and  $\rho_p$ , respectively, we have  $\rho = \rho_n + \rho_p$ ,  $\delta = (\rho_n - \rho_p)/\rho$ , and  $x = (\rho - \rho_0)/3\rho_0$ . In symmetric nuclear matter ( $\delta = 0$ ) at densities where  $|x| < 1$ , the density dependence of the EoS is controlled dominantly by  $K_0$ , while in neutron-rich matter ( $\delta \approx 1$ ) the EoS below and above  $\rho_0$  is largely driven by  $L$  and  $K_{\text{sym}}$ .

The saturation point as represented by the values of  $E_0$  and  $\rho_0$  is considered rather well known: Different theoretical assumptions lead to a maximal disagreement of the order of 1–2 MeV for  $E_0 \approx -16$  MeV [16] and 0.01–0.02 fm for  $\rho_0 \approx 0.16$  fm<sup>-3</sup> [17], i.e., roughly 12% at most. The uncertainty in  $J \approx 30$  MeV is of the order of a few MeV. Determining the EoS in the density region relevant for nuclei and neutron stars is then equivalent to determining the values of  $K_0$ ,  $L$  and  $K_{\text{sym}}$ . ( $Q_{\text{sym}}$  is also a relevant parameter but with a more marginal role [18, 19].) The above three parameters are poorly constrained.  $K_0$  is nonetheless best known among them: The empirically determined range is 200 – 260 MeV [17, 20]. A recent calculation based on microscopic theory predicts  $K_0 = 282$  MeV [21], which is one of the

largest values in the recent literature. The current status of  $L$  is summarized comprehensively in Ref. [15], where 24 new analyses of neutron stars give  $57.7 \pm 19$  MeV at 68% confidence level. The above range is consistent with the range  $L = 58.7 \pm 28.1$  MeV provided by a previous survey [13] and with the earlier empirical range  $L = 40 - 76$  MeV [17].

Compared with the above,  $K_{\text{sym}}$  is very poorly determined, with model estimates ranging from  $-400$  MeV to positive values [15]. Let us summarize how current constraints on  $K_{\text{sym}}$  have been obtained. A standard way is to identify correlations between  $K_{\text{sym}}$  and better-known model parameters, namely  $J$  and  $L$ , by surveying up to hundreds of models. A  $K_{\text{sym}}$  value is then deduced from the values of the other parameters. Recent works along this line propose  $K_{\text{sym}}$  values  $-112 \pm 71$  [22], and  $-100 \pm 100$  MeV [23]. Another way to obtain correlations among EoS parameters is to use effective field theories that provide a platform to calculate the correlations and uncertainties with realistic nuclear forces. A recent work obtains  $K_{\text{sym}} = -150$  to  $-70$  MeV [24], which is a result of correlation between  $K_{\text{sym}}$  and  $3J - L$  with appropriate ranges of  $J$  and  $L$ .

One may also identify correlations between model predictions for observables that can be measured and the EoS parameter of interest. One example is the relation of the energy of the giant monopole resonance with the nuclear incompressibility  $K_0$  [20]. As regards  $K_{\text{sym}}$ , recent works apply a Bayesian analysis to the tidal deformability of neutron stars. The results vary broadly and depend on the technical details and assumptions. For example Ref. [25] obtains  $K_{\text{sym}} = -113$  to  $-52$  MeV if  $L = 40 - 62$  MeV, and Ref. [6] gives  $K_{\text{sym}} = -374$  to  $45$  MeV. The 16 new analyses of neutron star observables in [15] suggest a range  $K_{\text{sym}} = -107 \pm 88$  MeV at 68% confidence level. This range excludes positive values, but the uncertainty is far larger than for  $K_0$  and  $L$ .

In a few cases  $K_{\text{sym}}$  is determined more directly from experiment. In Ref. [26], elliptic flow data are used to obtain allowed ranges of  $L$  and  $K_{\text{sym}}$ . The result is  $K_{\text{sym}} = 96 \pm 315(\text{exp}) \pm 170(\text{th}) \pm 166(\text{sys})$ . While elliptic flow data are obtained from experiments on Earth, astronomical data have also been used: In Ref. [4], the thermal emission from LMXB is analyzed, and the authors obtain  $K_{\text{sym}} = -155$  to  $-3$  MeV. The uncertainty in  $K_{\text{sym}}$  is significantly lower than in the elliptic-flow work, but at the same time the value of  $L$  was estimated to be  $37.2^{+9.2}_{-8.9}$  MeV, which is on the lower side of the generally accepted range.

Our poor knowledge of  $K_{\text{sym}}$  represents our poor knowledge of the EoS in the broad density domain necessary for the description of nuclei and neutron stars. Let us point out

also that most theoretical models providing input for the above analyses do not provide independent values for  $K_{\text{sym}}$ , but rather values strongly correlated with the dominant parameters  $J$  and  $L$  owing to a deficiency in independent model parameters. For a discussion pertaining to Skyrme models see, e.g., [27]. As exceptions besides *ab initio* calculations we may mention the meta-model [23], which however has minimal applicability at low densities and finite nuclei [28], and the KIDS (Korea-IBS-Daegu-SKKU) framework [18, 19, 27] for the nuclear EoS and energy density functional (EDF), which provides a unified approach to both nuclear-structure and astronomical types of data and is used in this work.

The KIDS EoS of homogeneous matter, specifically the energy per particle, has the analytical form

$$\mathcal{E}(\rho, \delta) = \mathcal{T}(\rho, \delta) + \sum_{i=0}^n c_i(\delta) \rho^{1+i/3}, \quad (4)$$

where  $\mathcal{T}$  is the kinetic energy per particle of a free Fermi gas and  $c_i(\delta)$  can be assumed quadratic to  $\delta$ . The expansion in terms of the cubic root of the density is informed by effective field theories and *ab initio* calculations and can accommodate any set of EoS parameters as defined in Eqs. (2), (3) [18, 29]. The EoS with the desired parameters is readily transposed to a nuclear EDF for finite nuclei with the additional freedom of choosing the values for the effective mass if desired [19, 30, 31]. In Ref. [27], we explored the density dependence of the symmetry energy in the KIDS framework by considering bulk properties of magic and open-shell nuclei and neutron-star properties. In particular, we explored the parameter space for  $(J, L, K_{\text{sym}})$  for a fixed EoS for symmetric matter,  $E_0 = -16$  MeV,  $\rho_0 = 0.16$  fm $^{-3}$ ,  $K_0 = 240$  MeV. The less relevant parameter  $Q_{\text{sym}}$  was fixed to 650 MeV. We also examined  $K_\tau$ , which is the droplet-model counterpart of  $K_{\text{sym}}$  and more appropriate for nuclei, by using the correspondence

$$K_\tau = K_{\text{sym}} - \left( 6 + \frac{Q_0}{K_0} \right) L. \quad (5)$$

Departures from existing model-dependent correlations between  $K_{\text{sym}}$  and  $J, L$  [22] were observed. Among other results, we concluded that  $K_{\text{sym}}$  is negative and no lower than  $-200$  MeV and suggested inconclusively  $-400$  to  $-300$  MeV as a range of likely values for  $K_\tau$ . In Ref. [32], the compression modulus  $K_0$  of symmetric nuclear matter was explored in a similar manner and the results were found consistent with the current literature.

In this work, we examine the acceptable values of  $K_{\text{sym}}$  by taking advantage of recent astronomical data from LMXB [3], GW170817 [7], GW190425 [9] and NICER [11]. We

explore both  $K_0$  and  $K_{\text{sym}}$  at the same time, as well as  $J$  and  $L$ . Note that in [27],  $K_0$  is fixed to 240 MeV, while in Ref. [32] the focus was on the uncertainties in  $J$  and  $L$ . Considering broadly accepted ranges for the four parameters  $K_0, J, L, K_{\text{sym}}$  (equivalently,  $K_\tau$  instead of  $K_{\text{sym}}$ ) independently of each other, the total number of EoSs examined initially is about 4000. Next, we select a fraction of them (roughly 10%) which describe bulk data of selected nuclei most precisely, use them to calculate neutron-star properties, and analyze the results. We evaluate correlation coefficients for the model parameters and predictions, revealing a strong correlation between  $K_{\text{sym}}$  and neutron star radii. By imposing all astronomical constraints at the same time, we deduce  $-150 < K_{\text{sym}} < 0$  MeV. We take the opportunity to comment also on the neutron skin thickness of  $^{208}\text{Pb}$  measured recently by the PREX collaboration [33].

The paper is organized as follows. In Sec. II we perform the first filtering of parameter sets using bulk nuclear data. In Sec. III, we analyze our calculations for neutron-star properties and compare them with the above-mentioned astronomical constraints. The 358 sets used at this stage and selected results are available as supplementary material. We provide a summary and perspectives in Sec. IV.

## II. EOS PARAMETERS AND CORRELATION ANALYSIS

The standard KIDS EoS has three free parameters for the EoS of symmetric nuclear matter ( $c_{i>2}(0) = 0$ ) and four for neutron matter, or equivalently the symmetry energy ( $c_{i>3}(1) = 0$ ) [18, 19]. This means that seven leading EoS parameters,  $(\rho_0, E_0, K_0)$  and  $(J, L, K_{\text{sym}}, Q_{\text{sym}})$ , can be controlled independently. Higher-order parameters such as  $Q_0$  do not vanish, but will fully depend on those seven. Although arbitrary extensions to any number of free parameters are straightforward, the use of seven low-order KIDS parameters has been found optimal and suffices for our purposes. As already mentioned, compared to  $K_0, J, L, K_{\text{sym}}$ , the saturation point  $(E_0, \rho_0)$  is quite accurately known and will be kept fixed at  $(-16 \text{ MeV}, 0.16 \text{ fm}^{-3})$ . As in [27], the less relevant parameter  $Q_{\text{sym}}$  will be kept fixed to the value of 650 MeV.

We begin by spanning the ranges  $K_0 = [230, 260]$  MeV,  $J = [30, 34]$  MeV,  $L = [40, 70]$  MeV,  $K_\tau = [-420, -240]$  MeV in increments of  $\Delta J = 0.5$  MeV,  $\Delta K_0 = \Delta L = 5$  MeV and  $\Delta K_\tau = 20$  MeV. In total, this gives us  $7 \times 9 \times 7 \times 10 = 4410$  EoS sets. At this stage,

we use  $K_\tau$  instead of  $K_{\text{sym}}$ , because we are examining finite nuclei. The relation between the two is straightforward, Eq. (5). For the present choices, the value of  $K_{\text{sym}}$  ranges from  $-300$  to  $96$  MeV. The  $Q_0$  value fully depends on  $K_0$  and for the present choices ranges from  $-373$  to  $-313$  MeV.

For each EoS, a KIDS-EDF is obtained, which has the form of an extended Skyrme functional [19, 27, 30, 31]. Besides the EoS parameters, the necessary additional EDF parameters, namely  $W_0$  (strength of spin-orbit force) and gradient terms represented by the Skyrme-like parameters  $t_1, t_2$ , are optimized by a fit to a few basic data [19, 30]. We note that the KIDS-EDF used at present has the simpler form given in Ref. [30], i.e., the exchange momentum-dependent terms  $y_{1,2} = t_{1,2}x_{1,2}$  are set to zero. The choice has no influence at all on our results for homogeneous matter, while any influence on bulk nuclear properties is too marginal to affect our current results [27, 31].

We then examine how accurately each EoS describes bulk nuclear properties by applying the corresponding EDF. As a measure of performance, we employ the average deviation per datum (ADPD) defined by

$$\text{ADPD}(N) \equiv \frac{1}{N} \sum_{i=1}^N \left| \frac{O_i^{\text{exp}} - O_i^{\text{cal}}}{O_i^{\text{exp}}} \right|, \quad (6)$$

where  $O_i^{\text{exp}}$  and  $O_i^{\text{cal}}$  denote the value of an observable from experiment and theory, respectively. Since the focus is on the EoS and not on nuclear structure, we will use only bulk properties of closed-shell nuclei. Specifically, we use  $N = 13$  data: binding energy [34] and charge radius [35] of  $^{16}\text{O}$ ,  $^{40}\text{Ca}$ ,  $^{48}\text{Ca}$ ,  $^{90}\text{Zr}$ ,  $^{132}\text{Sn}$ ,  $^{208}\text{Pb}$ , and binding energy of  $^{218}\text{U}$  [34]. The results are summarized in Fig. 1.

Roughly one tenth of all the EoSs give a value of ADPD less than 0.3% and will be examined further. The values of their parameters are available as supplementary material. The cutoff of 0.3% that we impose here is a rather stringent one. Values for the same ADPD(13) as provided by representative Skyrme functionals are given in Table I. Since those functionals are typically fitted to very different data, for comparison we also tabulate the values they give for 7 data only, namely the masses of  $^{16}\text{O}$ ,  $^{40}\text{Ca}$ ,  $^{48}\text{Ca}$ ,  $^{90}\text{Zr}$ ,  $^{132}\text{Sn}$ ,  $^{208}\text{Pb}$ , and  $^{218}\text{U}$ .

With each of the roughly 380 EoS sets selected, we calculate the neutron star EoS, solve the TOV equations, and obtain the mass-radius relations of the neutron star in a standard way [19, 27]. We are interested in particular in the radius  $R_{1.4}$  and tidal deformability  $\Lambda$  of

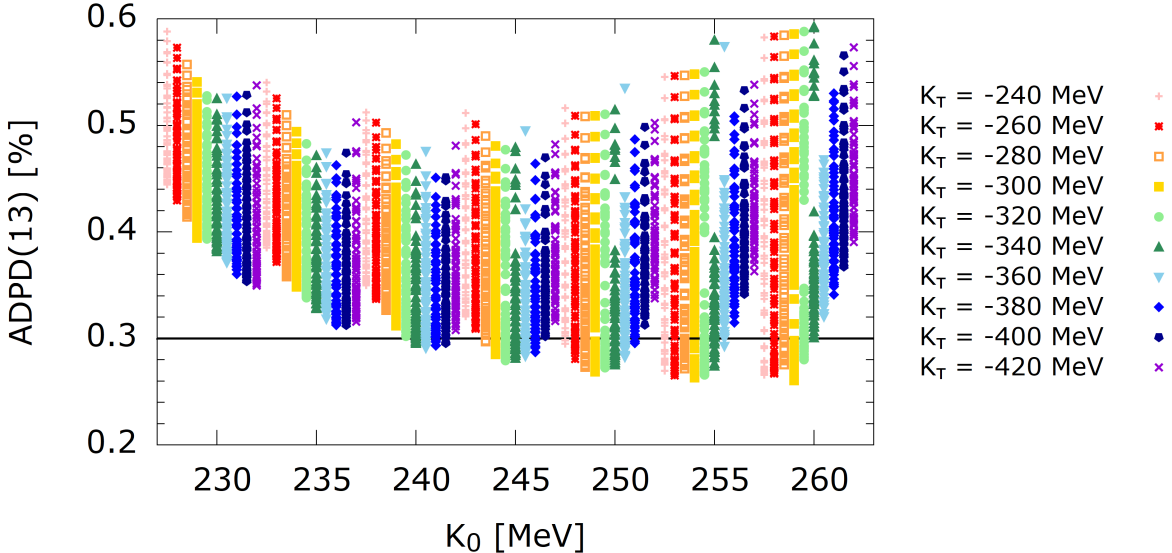


FIG. 1: Values of the criterion ADPD(13) with the examined sets of  $(K_0, J, L, K_\tau)$ . For each value of  $K_0$ , results with different  $K_\tau$  are shown displaced for visibility.

	SLy4	HFB9	SkM*	UNEDF0
ADPD(13)	0.86	0.87	0.84	0.98
ADPD(7)	0.30	0.36	0.38	0.59

TABLE I: ADPD(13), see Eq. (6), in units of percentage, calculated with representative Skyrme force models.

a canonical neutron star with a mass roughly equal to 1.4 solar masses and in the radius  $R_{2.0}$  of a two-solar mass neutron star. All sets predict the existence of such massive neutron stars.

Next, we evaluate the Pearson correlation coefficient  $r_{XY}$  between EoS parameters or predicted observables  $X, Y$

$$r_{XY} = \frac{\overline{XY} - \bar{X}\bar{Y}}{\sigma_X \sigma_Y}; \sigma_X = \sqrt{\overline{X^2} - \bar{X}^2} \quad (7)$$

and list the results in the lower triangle of Table II. The values will be updated to those of the upper triangle after we consider the astronomical observations in Sec. III. We include the quantity  $3J - L$ , whose correlation with  $K_{\text{sym}}$  has been discussed before, see Ref. [27] and

	$K_0$	$J$	$L$	$3J - L$	$K_{\text{sym}}$	$K_\tau$	$\Delta R_{\text{np}}$	$R_{1.4}$	$R_{2.0}$
$K_0$	1	-0.51	-0.24	<u>0.10</u>	0.35	0.50	-0.58	0.24	0.46
$J$	-0.39	1	0.56	-0.35	<u>-0.06</u>	-0.52	0.62	0.22	<u>0.01</u>
$L$	0.24	0.45	1	<b>-0.96</b>	0.50	-0.27	0.65	0.79	0.65
$3J - L$	-0.34	-0.27	<b>-0.98</b>		1	-0.60	0.14	-0.54	-0.84
$K_{\text{sym}}$	0.56	<u>0.09</u>	0.83	-0.88	1	0.69	-0.29	<b>0.90</b>	<b>0.91</b>
$K_\tau$	0.62	-0.30	0.34	-0.44	0.80	1	-0.85	0.33	0.43
$\Delta R_{\text{np}}$	-0.53	0.56	0.35	-0.26	-0.20	-0.70	1	<u>0.09</u>	<u>-0.05</u>
$R_{1.4}$	0.52	0.21	<b>0.91</b>	<b>-0.93</b>	<b>0.96</b>	0.66	<u>-0.02</u>	1	<b>0.97</b>
$R_{2.0}$	0.63	<u>0.09</u>	0.85	<b>-0.90</b>	<b>0.96</b>	0.69	-0.11	<b>0.99</b>	1

TABLE II: Correlation between the shown quantities according to Eq. (7). Lower triangle: Considering sets satisfying  $\text{ADPD}(13) < 0.3\%$ . Upper triangle: Considering sets which, in addition, satisfy selected astronomical constraints, see Sec. III.

references therein. Along with EoS parameters, we include the predictions for  $R_{1.4}$ ,  $R_{2.0}$ , and the neutron skin thickness of  $^{208}\text{Pb}$ . Note that adding  $Q_0$  to the table would offer no new information: Its correlation with all parameters would be the same as for  $K_0$  and exactly 1 between  $Q_0$  and  $K_0$ . That's because, with  $\rho_0$  and  $E_0$  fixed and having kept only three free parameters in the KIDS EoS of symmetric matter,  $Q_0$  is fully and linearly determined by  $K_0$ . In addition, the correlation of  $Q_{\text{sym}}$  with the other parameters is not defined, because we have kept its value fixed.

Numbers indicating strong (anti)correlation,  $|r_{XY}| \geq 0.9$ , are set in boldface, while those indicating absence of correlations,  $|r_{XY}| \leq 0.1$ , are set in underlined italics. Generally, the (anti)correlations between EoS parameters are weak at this stage, i.e., no linear correlations are apparent. Especially  $K_{\text{sym}}$  and  $J$  appear uncorrelated. Neutron star radii are strongly correlated with  $K_{\text{sym}}$  and to some extent  $L$  and  $3J - L$ . Notably, there are no correlations between the neutron skin thickness and the properties of neutron stars, in contrast with studies which focus on the role of  $L$  only [36].

All the tabulated numbers should be interpreted with some care. The parameters and results which have been used as data sets do not necessarily follow gaussian or symmetric

distributions, owing, for example, to the range cutoffs we have imposed in the EoS parameters, see also Fig. 1. Also, different values would be obtained if different data and acceptance criteria were used. Nevertheless, the highest and lowest values of  $|r_{XY}|$  marked in the table should carry some meaning. Also meaningful will be to inspect how the correlation patterns change or persist when we impose the neutron star constraints in the following.

### III. RESULTS FOR NEUTRON STARS

For the canonical neutron star,  $M = 1.4M_\odot$ , the common range of all the data for  $R_{1.4}$  from LMXB, GW170817 and GW109425 is roughly  $11.8 - 12.5$  km. A recent work based on Bayesian analysis reports that the upper limit of  $R_{1.4}$  will not exceed  $\sim 12.5$  km [37]. Therefore, we assume as acceptable a range of  $R_{1.4} = 11.8 - 12.5$  km. For  $R_{2.0}$  we only have the NICER measurement, taken for 2.08 solar masses, giving a much broader interval.

The results we obtained for neutron star radii for the sets satisfying the basic constraint from nuclear data, ADPD(13) < 0.3%, are shown as scatter plots in Fig. 2 along with relevant astronomical constraints. Specifically, in Fig. 2 (a) and (c) we show plots of  $R_{1.4}$  and  $R_{2.0}$ , respectively, against  $K_{\text{sym}}$  and in (b), a plot of  $R_{1.4}$  against  $3J - L$ . Both  $K_{\text{sym}}$  and  $3J - L$  were found strongly (anti)correlated with the radii (Table II, lower triangle). In order to reveal other possible systematics, in panels (a) and (c) we highlight the results for the highest and lowest values of  $L$  and in panel (b) we highlight values of  $J$ . All results are available as supplementary material.

Imposing the strictest possible criterion of  $11.8 \leq R_{1.4} \leq 12.5$  km, as mentioned above and indicated in Fig. 2(a), we obtain

$$-150 \leq K_{\text{sym}} \leq 0 \text{ MeV}.$$

Despite the varied range in  $K_0$  and the different nuclear data considered in this work, our results for  $K_{\text{sym}}$  remain perfectly consistent with those in Ref. [27], where we had deduced that  $-200 \leq K_{\text{sym}} \leq 0$  MeV. Let us note that we have also examined the dimensionless tidal deformability  $\Lambda_{1.4}$  of a canonical neutron star, which we evaluated as  $2.88 \times 10^{-6} R_{1.4}^{7.5}$  (with  $R_{1.4}$  in units of [km]) [39] and found strongly correlated with  $K_{\text{sym}}$ . For the EoS sets which satisfy the imposed radius constraints, one finds  $315 < \Lambda_{1.4} < 486$ , consistent with current estimates from the LIGO/Virgo measurements.

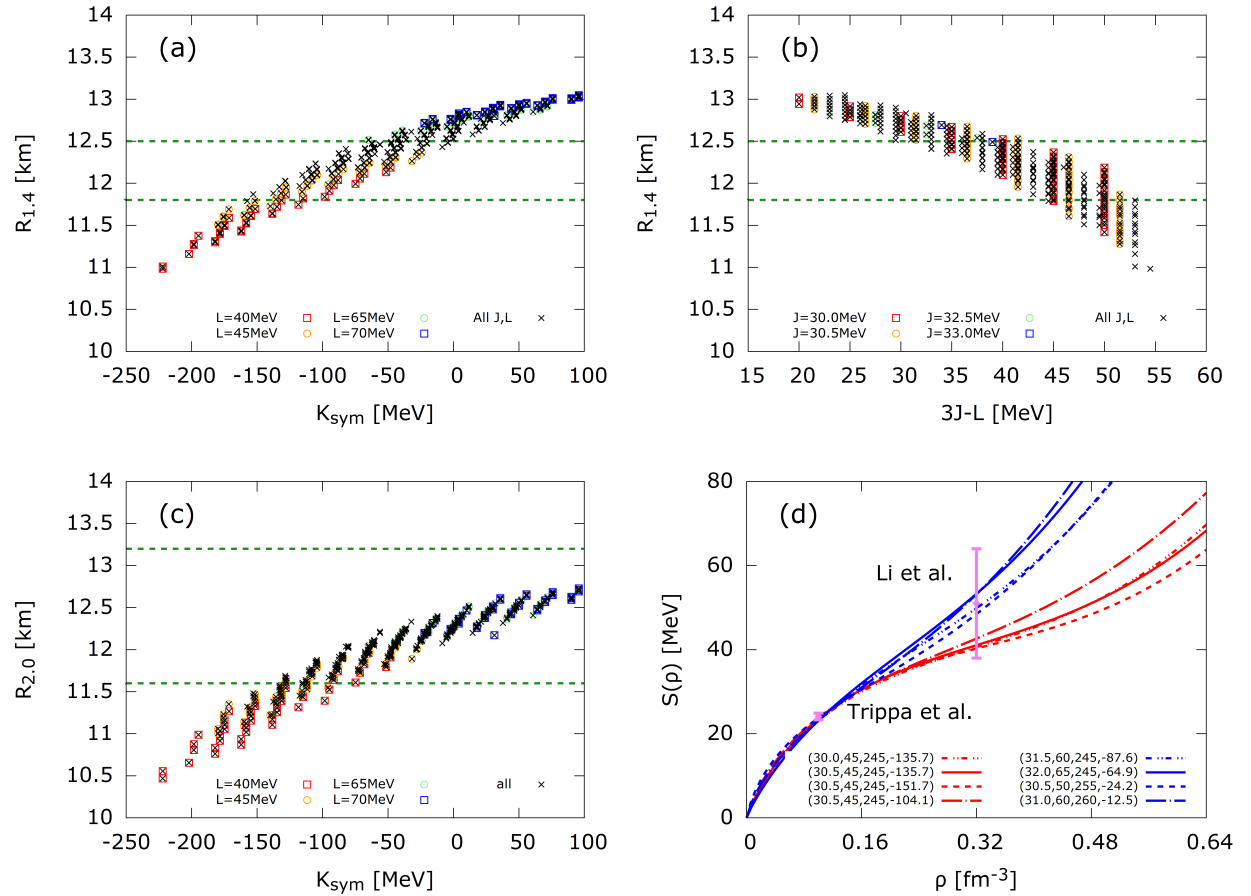


FIG. 2: (a)-(c): Predicted radii of neutron stars  $R_{1.4}$  (for 1.4 solar masses) and  $R_{2.0}$  (for 2.0 solar masses) shown against  $K_{\text{sym}}$  (a),(c) and  $3J - L$  (b) for all sets satisfying the basic constraint from nuclear data,  $\text{ADPD}(13) < 0.3\%$ . The dashed horizontal lines indicate combined astronomical constraints for the minimum and maximum acceptable values. (d): Symmetry energy corresponding to selected combinations of  $(J, L, K_0, K_{\text{sym}})$  values, indicated in units of MeV, roughly delimiting the allowed range based on the  $R_{1.4}$  constraint in (a). The shown constraint at  $0.1 \text{ fm}^{-3}$  (Trippa *et al.*) is from Ref. [38] and the estimate for  $S(2\rho_0)$  (Li *et al.*) is from Ref. [15].

A stratification with respect to  $L$  is apparent in Fig. 2(a) with lower radius values favoring generally lower values of  $L$ . Higher values of  $J$  are not favored. Overall, imposing again the strictest possible criterion of  $11.8 \leq R_{1.4} \leq 12.5$  km, as indicated in Figs. 2(b), gives us  $30 < 3J - L < 53$  MeV with  $J = 30 - 32$  MeV, implying roughly that

$$L < 3J - 30 \text{ MeV} < 66 \text{ MeV} , \quad L > 3J - 53 \text{ MeV} > 37 \text{ MeV}.$$

One may impose more lenient criteria to the constraint on  $R_{1.4}$ , given the uncertainty in all measurements. Then broader ranges would be obtained for the EoS parameters. What is clear from our analysis is that an accurate and precise measurement of a neutron star's mass would be instrumental in constraining the value of  $K_{\text{sym}}$  - more generally,  $S(\rho)$  at  $\rho > \rho_0$ .

In Fig. 2(d), we plot the symmetry energy corresponding to selected combinations of  $(J, L, K_0, K_{\text{sym}})$  values, indicated in units of MeV, roughly delimiting the allowed range based on the  $R_{1.4}$  constraint in (a). The upper curves correspond to  $R_{1.4}$  closer to the lower bound of 11.8 km while the lower curves correspond to  $R_{1.4}$  closer to the upper bound of 12.5 km. A crossing point is observed at roughly  $\rho = 0.1$  fm, which is roughly the average density in a heavy nucleus, consistently with other studies [12]. As indicated on the Figure, the value of  $S(0.1 \text{ fm}^{-3})$  is consistent with a constraint derived from giant dipole resonances [38]. The symmetry energy at two times the saturation density is obtained consistent with the range proposed in Ref. [15], which was extracted from a variety of heavy-ion collision data and astronomical data.

An important observation is that in all cases the symmetry energy shows an inflection point at some density above saturation, i.e., the curvature changes sign from negative to positive. This behavior is mathematically possible because the higher-order parameters such as  $Q_{\text{sym}}$  do not vanish in this scheme. The inflection point is found here consistently within the interval between  $\rho_0$  and  $2\rho_0$ .

The above constraints are based solely on bulk nuclear properties and existing astronomical data. We take the opportunity to comment on the neutron skin thickness of the nucleus  $^{208}\text{Pb}$ , which was extracted recently from parity violating electron scattering by the PREX collaboration [33] and found larger than expected from earlier estimates and known systematics [40, 41]. It is generally thought that a moderate value of  $L$ , such as extracted also in this work, does not favor a thick neutron skin. However, presently we find a rather weak correlation of the neutron skin thickness with  $L$  compared with a much stronger anti-correlation with  $K_\tau$ . A thorough investigation of  $K_\tau$  is therefore called for and is currently in progress.

Let us further inspect a few EoS sets obtained here which satisfy the astronomical constraints defined in Fig. 2 but also give a  $\Delta R_{np}$  prediction for  $^{208}\text{Pb}$  consistent with both the first PREX measurement,  $0.33^{+0.16}_{-0.18}$  fm [42], and an earlier broad estimate  $0.195 \pm 0.057$  fm [40]. In Fig. 3 we plot the density dependence of the symmetry energy for

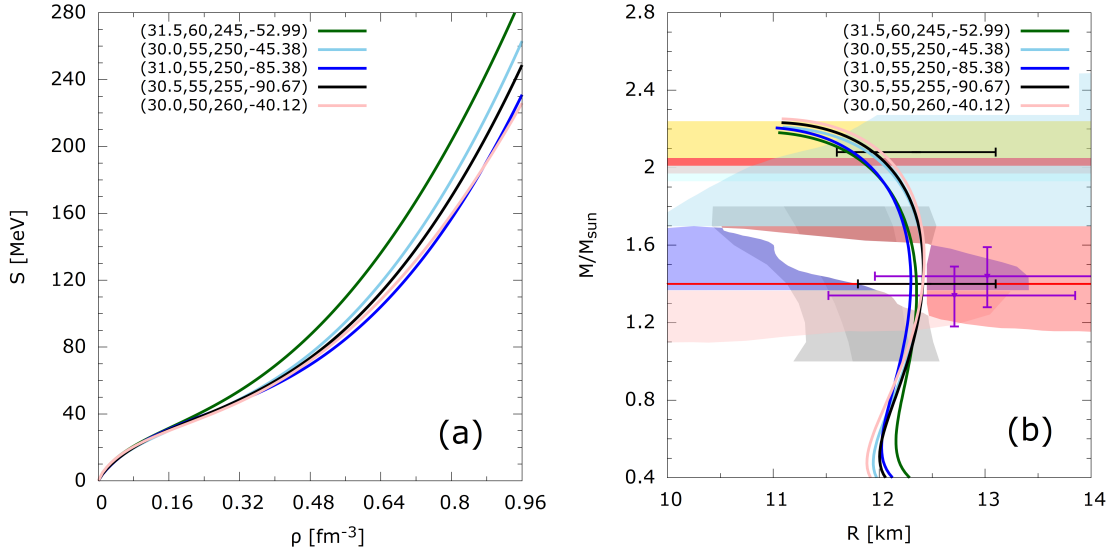


FIG. 3: Symmetry energy (a) and neutron star mass-radius curves (b) for representative EoSs satisfying astronomical and neutron-skin data as discussed in the text. The labels show the values of  $(L, J, K_0, K_{\text{sym}})$  in units of MeV.

five such sets (a) and the resulting neutron-star mass-radius relations (b). (One of the EoSs is consistent also with the PREX-II measurement by giving  $\Delta R_{np} = 0.212$  fm.) Astronomical constraints from various sources are displayed in Fig. 3(b) related to masses observed or to masses and radii of neutron stars [2, 3, 5, 7, 9, 10, 43, 44]. What we conclude from this picture, compared to Fig. 2(d), is that combining both nuclear data (sub-saturation regime) and astronomical data (high-density regime) it becomes possible to constrain significantly the density dependence of the nuclear symmetry energy. Precise astronomical data and more conclusive measurements of the neutron skin thickness are required.

#### IV. SUMMARY

In this work, we attempt to constrain the curvature parameter of the symmetry energy  $K_{\text{sym}}$  based on bulk nuclear properties and available astronomical data. We utilize the KIDS framework for the nuclear EoS and EDF, which imposes no *a priori*, spurious correlations among EoS parameters. Assuming a standard saturation point, we calculate bulk nuclear properties within KIDS-EDF for different values of the compression modulus of symmetric nuclear matter ( $K_0$ ) and of the leading-order symmetry energy parameters, i.e., the symme-

try energy ( $J$ ) and slope ( $L$ ) at saturation density, each within a broadly accepted range, as well as  $K_{\text{sym}}$ . The skewness parameter ( $Q_{\text{sym}}$ ) is presently kept fixed at 650 MeV. For all EoS parameter sets which describe the selected nuclear data within better than 0.3%, we calculate the neutron-star equation of state and mass-radius relation and analyze the results in terms of Pearson correlation coefficients  $r$ .

The curvature parameter is found strongly correlated with neutron-star radii. By imposing that available measurements of neutron star radii must be reproduced within their given uncertainties, we arrive at an acceptable value of  $K_{\text{sym}}$  between roughly  $-150$  and zero MeV. The symmetry energy consistently shows an inflection point at densities between  $\rho_0$  and  $2\rho_0$ . Stronger constraints would be possible with more precise astronomical data. The neutron skin thickness of  $^{208}\text{Pb}$  shows no correlation at all with neutron star radii, but precise measurements would be useful for constraining the symmetry energy at sub-saturation densities, further aiding the evaluation of  $K_{\text{sym}}$ .

### Acknowledgments

This work was supported by the National Research Foundation of Korea (NRF) grant funded by the Korea govenment (No. 2018R1A5A1025563 and No. 2020R1F1A1052495) and by the Rare Isotope Science Project of the Institute for Basic Science funded by the Ministry of Science, ICT and Future Planning and the National Research Foundation (NRF) of Korea (2013M7A1A1075764).

- [1] P. B. Demorest, T. Pennucci, S. M. Ransom, M. S. E. Roberts, and J. W. T. Hessels, Nature (London) **467**, 1081 (2010), 1010.5788.
- [2] H. T. Cromartie et al., Nature Astronomy **4**, 72 (2020).
- [3] A. W. Steiner, J. M. Lattimer, and E. F. Brown, Astrophys. J. **722**, 33 (2010).
- [4] N. B. d'Etivaux, S. Guillot, J. Margueron, N. Webb, M. Catelan, and A. Reisenegger, Astrophys. J. **887**, 48 (2019).
- [5] J. Antoniadis et al., Science **340**, 1233232 (2013).
- [6] C. A. Raithel and F. Özel, Astrophys. J. **885**, 121 (2019).

- [7] B. P. Abbott et al. (The LIGO Scientific Collaboration and the Virgo Collaboration), Phys. Rev. Lett. **121**, 161101 (2018).
- [8] B. P. Abbott et al. (LIGO Scientific Collaboration and Virgo Collaboration), Phys. Rev. Lett. **119**, 161101 (2017).
- [9] B. P. Abbott et al., Astrophys. J. **892**, L3 (2020).
- [10] T. E. Riley et al., Astrophys. J. **887**, L21 (2019).
- [11] M. C. Miller et al. (2021), arXiv: 2105.06979.
- [12] M. Baldo and G. Burgio, Prog. Part. Nucl. Phys. **91**, 203 (2016).
- [13] M. Oertel, M. Hempel, T. Klähn, and S. Typel, Rev. Mod. Phys. **89**, 015007 (2017).
- [14] J. W. Holt and Y. Lim, Physics Letters B **784**, 77 (2018).
- [15] B.-A. Li, B.-J. Cai, W.-J. Xie, and N.-B. Zhang, Universe **7**, 182 (2021).
- [16] M. C. Atkinson, W. H. Dickhoff, M. Piarulli, A. Rios, and R. B. Wiringa, Phys. Rev. C **102**, 044333 (2020).
- [17] M. Dutra, O. Lourenço, J. S. Sá Martins, A. Delfino, J. R. Stone, and P. D. Stevenson, Phys. Rev. C **85**, 035201 (2012).
- [18] P. Papakonstantinou, T.-S. Park, Y. Lim, and C. H. Hyun, Phys. Rev. C **97**, 014312 (2018).
- [19] H. Gil, Y.-M. Kim, C. H. Hyun, P. Papakonstantinou, and Y. Oh, Phys. Rev. C **100**, 014312 (2019).
- [20] U. Garg and G. Colò, Prog. Part. Nucl. Phys. **101**, 55 (2018).
- [21] L. Brandes, N. Kaiser, and W. Weise, Eur. Phys. J. A **57**, 243 (2021).
- [22] C. Mondal, B. K. Agrawal, J. N. De, S. K. Samaddar, M. Centelles, and X. Viñas, Phys. Rev. C **96**, 021302 (2017).
- [23] J. Margueron, R. Hoffmann Casali, and F. Gulminelli, Phys. Rev. C **97**, 025805 (2018).
- [24] Y. Lim and J. W. Holt, Eur. Phys. J. A **55**, 209 (2019).
- [25] T. Malik, N. Alam, M. Fortin, C. Providência, B. K. Agrawal, T. K. Jha, B. Kumar, and S. K. Patra, Phys. Rev. C **98**, 035804 (2018).
- [26] M. D. Cozma, Eur. Phys. J. A **54**, 40 (2018).
- [27] H. Gil, Y.-M. Kim, P. Papakonstantinou, and C. H. Hyun, Phys. Rev. C **103**, 034330 (2021).
- [28] D. Chatterjee, F. Gulminelli, A. R. Raduta, and J. Margueron, Phys. Rev. C **96**, 065805 (2017).
- [29] P. Papakonstantinou and H. Gil, HNPS Advances in Nuclear Physics, [S.l.] **26**, 104 (2018).

- [30] H. Gil, Y. Oh, C. H. Hyun, and P. Papakonstantinou, New Physics: Sae Mulli **67**, 456 (2017).
- [31] H. Gil, P. Papakonstantinou, C. H. Hyun, and Y. Oh, Phys. Rev. C **99**, 064319 (2019).
- [32] H. Gil and C. H. Hyun, New Physics: Sae Mulli **71**, 242 (2021).
- [33] D. Adhikari et al. (PREX Collaboration), Phys. Rev. Lett. **126**, 172502 (2021).
- [34] National Nuclear Data Center, Brookhaven National Laboratory, [www.nndc.bnl.gov/nudat2/](http://www.nndc.bnl.gov/nudat2/).
- [35] I. Angeli and K. Marinova, Atomic Data and Nuclear Data Tables **99**, 69 (2013).
- [36] B. T. Reed, F. J. Fattoyev, C. J. Horowitz, and J. Piekarewicz, Phys. Rev. Lett. **126**, 172503 (2021).
- [37] M. Kim, Y.-M. Kim, K. H. Sung, C.-H. Lee, and K. Kwak, A and A **650**, A139 (2021).
- [38] L. Trippa, G. Colò, and E. Vigezzi, Phys. Rev. C **77**, 061304 (2008).
- [39] E. Annala, T. Gorda, A. Kurkela, and A. Vuorinen, Phys. Rev. Lett. **120**, 172703 (2018).
- [40] X. Roca-Maza, M. Centelles, X. Viñas, and M. Warda, Phys. Rev. Lett. **106**, 252501 (2011).
- [41] J. Piekarewicz, Phys. Rev. C **104**, 024329 (2021).
- [42] S. Abrahamyan et al. (PREX Collaboration), Phys. Rev. Lett. **108**, 112502 (2012).
- [43] M. C. Miller et al., Astrophys. J. **887**, L24 (2019).
- [44] M. C. Miller et al., Astrophys. J. **918**, L28 (2021).

## Supplementary material

Values of parameters and results analysed in this work are tabulated below. The EoS parameters  $K_0$ ,  $J$ ,  $L$ ,  $K_{\text{sym}}$  and the droplet parameter  $K_\tau$  are given in units of MeV. The average deviation per datum ADPD(13) for 13 data (see Eq. (6) of the main text) is given in percentage points %. The spin-orbit and momentum-term couplings  $W_0, t_1, t_2$  and the surface parameters  $C_{12} = \frac{1}{64}[-9t_1 + 5t_2]$ ,  $D_{12} = \frac{1}{64}[3t_1 + t_2]$  are given in units of MeV fm<sup>5</sup>. For the above parameters, typical values for the isoscalar and isovector nucleon effective masses are, respectively, 0.98 and 0.82 times the bare nucleon mass (with some deviations).  $M_1 \approx 1.4M_\odot$  (more precisely in the range  $(1.39 - 1.41)M_\odot$ ) denotes the mass of a canonical neutron star and  $M_2 = 2.0M_\odot$  that of a massive star. The respective radii,  $R_{M_1}$  and  $R_{M_2}$  are given in units of km. The neutron skin thickness of <sup>208</sup>Pb,  $\Delta R_{np}$ , is given in units of fm.

$K_0$	$Q_0$	$J$	$L$	$K_\tau$	$K_{\text{sym}}$	ADPD(13)	$W_0$	$t_1$	$t_2$	$C_{12}$	$D_{12}$	$R_{M_1}$	$R_{M_2}$	$\Delta R_{np}$
240	-372.65	30.5	40	-340	-162.11	0.298	100.82	293.18	-172.48	-54.70	11.05	11.44	10.94	0.164
240	-372.65	30.5	40	-360	-182.11	0.296	98.44	291.85	-172.81	-54.54	10.98	11.31	10.83	0.174
240	-372.65	31.0	40	-340	-162.11	0.297	104.91	294.50	-172.28	-54.87	11.11	11.43	10.87	0.163
240	-372.65	31.0	45	-340	-139.87	0.295	102.06	293.40	-172.49	-54.73	11.06	11.73	11.22	0.171
240	-372.65	31.0	40	-360	-182.11	0.291	102.70	292.57	-172.84	-54.65	11.01	11.30	10.76	0.173
240	-372.65	31.0	45	-360	-159.87	0.293	99.58	291.99	-172.84	-54.56	10.99	11.62	11.14	0.181
240	-372.65	31.0	40	-380	-202.11	0.293	100.08	291.62	-173.03	-54.53	10.97	11.16	10.65	0.183
240	-372.65	31.0	45	-380	-179.87	0.297	97.14	291.21	-172.97	-54.47	10.95	11.51	11.06	0.192
240	-372.65	31.0	40	-400	-222.11	0.295	97.64	291.00	-173.08	-54.44	10.94	11.01	10.56	0.194
240	-372.65	31.5	50	-340	-117.63	0.296	103.23	293.61	-172.51	-54.77	11.07	11.97	11.45	0.178
240	-372.65	31.5	55	-340	-95.40	0.300	100.28	292.77	-172.62	-54.66	11.03	12.17	11.67	0.186
240	-372.65	31.5	45	-360	-159.87	0.298	103.66	292.74	-172.87	-54.67	11.02	11.62	11.09	0.180
240	-372.65	31.5	50	-360	-137.63	0.296	100.73	292.14	-172.89	-54.59	10.99	11.88	11.38	0.188
240	-372.65	31.5	55	-360	-115.40	0.298	97.68	291.64	-172.87	-54.52	10.97	12.10	11.61	0.197
240	-372.65	31.5	45	-380	-179.87	0.293	101.67	291.97	-173.20	-54.59	10.98	11.50	11.01	0.190
240	-372.65	31.5	50	-380	-157.63	0.298	98.23	291.32	-173.01	-54.48	10.95	11.79	11.32	0.199
240	-372.65	31.5	40	-400	-222.11	0.297	102.09	291.69	-173.32	-54.56	10.96	10.98	10.47	0.192
240	-372.65	32.0	55	-360	-115.40	0.299	101.85	292.30	-172.93	-54.62	11.00	12.10	11.59	0.195
245	-357.65	30.0	40	-280	-98.39	0.297	100.69	262.88	-181.08	-51.12	9.49	11.84	11.39	0.137
245	-357.65	30.0	40	-300	-118.39	0.294	108.07	337.85	-152.07	-59.39	13.46	11.75	11.32	0.136
245	-357.65	30.0	40	-320	-138.39	0.288	101.18	298.50	-166.96	-55.02	11.38	11.64	11.22	0.151
245	-357.65	30.0	45	-320	-115.69	0.299	98.20	295.63	-167.89	-54.69	11.23	11.90	11.51	0.160
245	-357.65	30.0	40	-340	-158.39	0.289	98.33	293.02	-168.92	-54.40	11.10	11.53	11.12	0.162
245	-357.65	30.0	45	-340	-135.69	0.300	95.53	291.86	-169.17	-54.26	11.04	11.81	11.44	0.170
245	-357.65	30.0	40	-360	-178.39	0.295	95.85	290.72	-169.62	-54.13	10.98	11.42	11.04	0.173
245	-357.65	30.5	50	-280	-52.99	0.298	97.38	246.51	-187.42	-49.31	8.63	12.26	11.83	0.154

245 -357.65 30.5 45 -300 -95.69	0.288	111.74 357.10 -144.87 -61.53 14.48 11.98 11.55 0.141
245 -357.65 30.5 50 -300 -72.99	0.297	103.84 313.52 -161.29 -56.69 12.18 12.19 11.77 0.154
245 -357.65 30.5 40 -320 -138.39	0.279	105.91 305.24 -164.68 -55.79 11.73 11.64 11.17 0.150
245 -357.65 30.5 45 -320 -115.69	0.282	102.59 299.47 -166.70 -55.14 11.43 11.90 11.48 0.158
245 -357.65 30.5 50 -320 -92.99	0.292	99.53 296.26 -167.75 -54.77 11.27 12.11 11.71 0.158
245 -357.65 30.5 40 -340 -158.39	0.281	102.55 295.03 -168.46 -54.65 11.20 11.53 11.07 0.161
245 -357.65 30.5 45 -340 -135.69	0.286	99.67 293.38 -168.87 -54.45 11.11 11.81 11.40 0.169
245 -357.65 30.5 50 -340 -112.99	0.294	96.74 292.15 -169.14 -54.30 11.05 12.04 11.64 0.178
245 -357.65 30.5 40 -360 -178.39	0.283	99.95 291.81 -169.51 -54.28 11.03 11.41 10.97 0.172
245 -357.65 30.5 45 -360 -155.69	0.291	97.08 290.93 -169.62 -54.16 10.99 11.71 11.31 0.180
245 -357.65 30.5 50 -360 -132.99	0.300	94.19 290.24 -169.71 -54.07 10.95 11.96 11.57 0.189
245 -357.65 30.5 40 -380 -198.39	0.287	97.50 290.17 -169.98 -54.08 10.95 11.28 10.88 0.182
245 -357.65 30.5 45 -380 -175.69	0.296	94.58 289.59 -169.98 -54.00 10.92 11.61 11.23 0.191
245 -357.65 31.0 50 -300 -72.99	0.287	117.97 398.96 -129.21 -66.20 16.68 12.19 11.75 0.142
245 -357.65 31.0 55 -300 -50.29	0.293	105.68 318.19 -159.61 -57.21 12.42 12.37 11.92 0.160
245 -357.65 31.0 40 -320 -138.39	0.293	112.34 325.96 -157.06 -58.11 12.83 11.64 11.11 0.146
245 -357.65 31.0 45 -320 -115.69	0.285	107.49 307.42 -163.97 -56.04 11.85 11.90 11.44 0.156
245 -357.65 31.0 50 -320 -92.99	0.284	104.01 300.57 -166.39 -55.27 11.49 12.12 11.69 0.165
245 -357.65 31.0 55 -320 -70.29	0.287	100.83 296.93 -167.59 -54.85 11.30 12.30 11.87 0.173
245 -357.65 31.0 40 -340 -158.39	0.290	106.81 298.11 -167.57 -55.01 11.36 11.52 11.02 0.160
245 -357.65 31.0 45 -340 -135.69	0.284	103.86 295.55 -168.35 -54.71 11.22 11.81 11.37 0.168
245 -357.65 31.0 50 -340 -112.99	0.287	100.95 293.78 -168.83 -54.50 11.13 12.04 11.62 0.176
245 -357.65 31.0 55 -340 -90.29	0.290	97.96 292.45 -169.11 -54.34 11.07 12.24 11.82 0.185
245 -357.65 31.0 60 -340 -67.59	0.298	94.95 291.43 -169.31 -54.21 11.02 12.41 11.98 0.193
245 -357.65 31.0 40 -360 -178.39	0.287	104.06 293.18 -169.29 -54.45 11.10 11.40 10.92 0.170
245 -357.65 31.0 45 -360 -155.69	0.286	101.20 292.08 -169.50 -54.32 11.04 11.71 11.28 0.179
245 -357.65 31.0 50 -360 -132.99	0.289	98.35 291.21 -169.65 -54.21 11.00 11.96 11.55 0.187
245 -357.65 31.0 55 -360 -110.29	0.294	95.34 290.44 -169.72 -54.10 10.96 12.17 11.76 0.196
245 -357.65 31.0 40 -380 -198.39	0.291	101.56 291.02 -169.94 -54.20 10.99 11.27 10.81 0.181
245 -357.65 31.0 45 -380 -175.69	0.293	98.68 290.35 -169.99 -54.11 10.95 11.60 11.19 0.189
245 -357.65 31.0 50 -380 -152.99	0.295	95.73 289.75 -170.01 -54.03 10.93 11.87 11.48 0.198
245 -357.65 31.5 60 -300 -27.59	0.294	107.69 324.68 -157.22 -57.94 12.76 12.53 12.05 0.166
245 -357.65 31.5 65 -300 -4.89	0.298	102.71 306.80 -163.87 -55.95 11.82 12.67 12.18 0.177
245 -357.65 31.5 50 -320 -92.99	0.294	109.08 310.08 -163.05 -56.34 11.99 12.12 11.65 0.163
245 -357.65 31.5 55 -320 -70.29	0.287	105.40 301.82 -166.02 -55.41 11.55 12.31 11.85 0.172
245 -357.65 31.5 60 -320 -47.59	0.289	102.11 297.68 -167.40 -54.94 11.34 12.47 12.01 0.180
245 -357.65 31.5 65 -320 -24.89	0.292	98.92 295.13 -168.17 -54.64 11.21 12.62 12.13 0.189
245 -357.65 31.5 70 -320 -2.18	0.298	95.75 293.36 -168.62 -54.43 11.12 12.75 12.25 0.198
245 -357.65 31.5 50 -340 -112.99	0.290	105.21 296.14 -168.26 -54.79 11.25 12.04 11.59 0.175
245 -357.65 31.5 55 -340 -90.29	0.289	102.17 294.19 -168.76 -54.56 11.15 12.24 11.79 0.183
245 -357.65 31.5 60 -340 -67.59	0.292	99.14 292.78 -169.09 -54.38 11.08 12.42 11.96 0.192
245 -357.65 31.5 65 -340 -44.89	0.294	96.08 291.69 -169.30 -54.24 11.03 12.57 12.10 0.201
245 -357.65 31.5 45 -360 -155.69	0.294	105.32 293.53 -169.26 -54.50 11.11 11.71 11.24 0.177
245 -357.65 31.5 50 -360 -132.99	0.289	102.44 292.37 -169.50 -54.36 11.06 11.96 11.52 0.186

245	-357.65	31.5	55	-360	-110.29	0.292	99.51	291.44	-169.65	-54.24	11.01	12.17	11.74	0.194
245	-357.65	31.5	60	-360	-87.59	0.294	96.47	290.65	-169.73	-54.13	10.97	12.35	11.92	0.203
245	-357.65	31.5	65	-360	-64.89	0.299	93.35	289.96	-169.77	-54.04	10.94	12.51	12.05	0.212
245	-357.65	31.5	45	-380	-175.69	0.299	102.80	291.26	-169.96	-54.24	11.00	11.60	11.14	0.188
245	-357.65	31.5	50	-380	-152.99	0.299	99.86	290.55	-170.01	-54.14	10.96	11.87	11.44	0.196
245	-357.65	32.0	65	-300	-4.89	0.294	110.10	334.38	-153.63	-59.02	13.27	12.68	12.17	0.172
245	-357.65	32.0	70	-300	17.82	0.298	104.17	309.37	-162.97	-56.24	11.96	12.81	12.28	0.183
245	-357.65	32.0	60	-320	-47.59	0.293	106.77	303.26	-165.56	-55.58	11.63	12.48	11.99	0.178
245	-357.65	32.0	65	-320	-24.89	0.292	103.36	298.50	-167.18	-55.04	11.38	12.63	12.12	0.187
245	-357.65	32.0	70	-320	-2.18	0.294	100.12	295.68	-168.04	-54.71	11.23	12.76	12.23	0.196
245	-357.65	32.0	55	-340	-90.29	0.298	106.47	296.74	-168.11	-54.86	11.28	12.25	11.77	0.181
245	-357.65	32.0	60	-340	-67.59	0.292	103.41	294.64	-168.70	-54.61	11.18	12.42	11.94	0.190
245	-357.65	32.0	65	-340	-44.89	0.294	100.31	293.13	-169.05	-54.43	11.10	12.57	12.08	0.199
245	-357.65	32.0	70	-340	-22.18	0.297	97.19	291.96	-169.28	-54.28	11.04	12.71	12.20	0.208
245	-357.65	32.0	55	-360	-110.29	0.295	103.65	292.67	-169.48	-54.40	11.07	12.17	11.71	0.192
245	-357.65	32.0	60	-360	-87.59	0.295	100.66	291.69	-169.65	-54.27	11.02	12.36	11.88	0.201
245	-357.65	32.0	65	-360	-64.89	0.299	97.56	290.84	-169.73	-54.16	10.98	12.52	12.03	0.210
245	-357.65	32.5	70	-300	17.82	0.294	113.23	350.51	-147.60	-60.82	14.12	12.81	12.26	0.176
245	-357.65	32.5	70	-320	-2.18	0.295	104.60	299.42	-166.92	-55.15	11.43	12.77	12.23	0.194
245	-357.65	32.5	65	-340	-44.89	0.298	104.60	295.13	-168.62	-54.68	11.20	12.58	12.06	0.197
245	-357.65	32.5	70	-340	-22.18	0.297	101.44	293.48	-169.01	-54.48	11.12	12.72	12.18	0.205
250	-342.65	30.0	45	-240	-31.68	0.295	104.75	273.25	-173.89	-52.01	10.09	12.26	11.89	0.122
250	-342.65	30.0	50	-240	-8.53	0.295	102.17	271.48	-174.40	-51.80	10.00	12.43	12.08	0.129
250	-342.65	30.0	40	-260	-74.82	0.289	104.76	269.69	-175.31	-51.62	9.90	11.99	11.61	0.125
250	-342.65	30.0	45	-260	-51.68	0.281	102.01	266.39	-176.41	-51.24	9.73	12.20	11.83	0.132
250	-342.65	30.0	50	-260	-28.53	0.290	98.95	261.25	-178.23	-50.66	9.46	12.37	12.02	0.140
250	-342.65	30.0	40	-280	-94.82	0.275	100.79	253.29	-181.54	-49.80	9.04	11.91	11.52	0.136
250	-342.65	30.0	45	-280	-71.68	0.273	95.62	232.52	-189.51	-47.50	7.94	12.12	11.77	0.147
250	-342.65	30.0	40	-300	-114.82	0.269	121.35	440.33	-110.21	-70.53	18.92	11.82	11.44	0.122
250	-342.65	30.0	45	-300	-91.68	0.277	106.36	332.76	-150.53	-58.56	13.25	12.05	11.70	0.142
250	-342.65	30.0	50	-300	-68.53	0.284	101.30	312.31	-158.17	-56.28	12.17	12.24	11.90	0.152
250	-342.65	30.0	55	-300	-45.38	0.294	97.61	303.55	-161.34	-55.29	11.71	12.41	12.07	0.161
250	-342.65	30.0	40	-320	-134.82	0.273	103.35	304.49	-161.38	-55.43	11.75	11.72	11.34	0.148
250	-342.65	30.0	45	-320	-111.68	0.280	100.18	299.36	-163.17	-54.85	11.48	11.97	11.63	0.156
250	-342.65	30.0	50	-320	-88.53	0.288	97.14	296.06	-164.25	-54.46	11.31	12.17	11.84	0.165
250	-342.65	30.0	40	-340	-154.82	0.277	99.99	294.30	-165.13	-54.29	11.22	11.62	11.26	0.160
250	-342.65	30.0	45	-340	-131.68	0.284	97.17	292.52	-165.64	-54.08	11.12	11.88	11.56	0.168
250	-342.65	30.0	50	-340	-108.53	0.298	94.29	291.10	-165.98	-53.90	11.05	12.10	11.78	0.176
250	-342.65	30.0	40	-360	-174.82	0.282	97.34	290.46	-166.45	-53.85	11.01	11.51	11.16	0.171
250	-342.65	30.0	45	-360	-151.68	0.295	94.53	289.48	-166.63	-53.73	10.97	11.79	11.47	0.179
250	-342.65	30.5	55	-240	14.62	0.295	103.67	272.16	-174.26	-51.89	10.03	12.58	12.20	0.135
250	-342.65	30.5	60	-240	37.77	0.299	100.92	270.00	-174.92	-51.63	9.92	12.72	12.32	0.143
250	-342.65	30.5	45	-260	-51.68	0.300	106.33	270.57	-175.10	-51.73	9.95	12.20	11.81	0.131
250	-342.65	30.5	50	-260	-28.53	0.289	103.58	267.63	-176.05	-51.39	9.79	12.38	12.00	0.138

250	-342.65	30.5	55	-260	-5.38	0.286	100.56	263.21	-177.59	-50.89	9.56	12.53	12.15	0.146
250	-342.65	30.5	60	-260	17.77	0.294	97.06	255.62	-180.35	-50.04	9.16	12.67	12.29	0.155
250	-342.65	30.5	45	-280	-71.68	0.287	102.65	256.79	-180.30	-50.20	9.22	12.13	11.75	0.143
250	-342.65	30.5	50	-280	-48.53	0.278	98.19	241.58	-186.06	-48.51	8.42	12.31	11.94	0.152
250	-342.65	30.5	50	-300	-68.53	0.274	109.38	346.48	-145.43	-60.09	13.97	12.25	11.88	0.147
250	-342.65	30.5	55	-300	-45.38	0.280	103.16	316.75	-156.57	-56.78	12.40	12.42	12.06	0.158
250	-342.65	30.5	60	-300	-22.23	0.287	99.12	305.75	-160.59	-55.54	11.82	12.57	12.20	0.168
250	-342.65	30.5	65	-300	0.91	0.297	95.66	299.95	-162.62	-54.88	11.52	12.71	12.32	0.177
250	-342.65	30.5	40	-320	-134.82	0.272	108.96	318.57	-156.30	-57.01	12.49	11.72	11.31	0.146
250	-342.65	30.5	45	-320	-111.68	0.275	105.00	306.83	-160.60	-55.69	11.87	11.97	11.60	0.155
250	-342.65	30.5	50	-320	-88.53	0.277	101.67	300.77	-162.74	-55.01	11.56	12.18	11.82	0.163
250	-342.65	30.5	55	-320	-65.38	0.283	98.55	297.02	-163.99	-54.58	11.36	12.36	12.00	0.172
250	-342.65	30.5	60	-320	-42.23	0.292	95.48	294.43	-164.79	-54.28	11.23	12.52	12.15	0.180
250	-342.65	30.5	40	-340	-154.82	0.275	104.31	297.69	-164.14	-54.69	11.39	11.61	11.21	0.158
250	-342.65	30.5	45	-340	-131.68	0.277	101.42	295.03	-164.97	-54.38	11.25	11.88	11.52	0.166
250	-342.65	30.5	50	-340	-108.53	0.279	98.52	293.08	-165.53	-54.15	11.15	12.10	11.76	0.175
250	-342.65	30.5	55	-340	-85.38	0.288	95.59	291.56	-165.91	-53.96	11.07	12.29	11.94	0.183
250	-342.65	30.5	40	-360	-174.82	0.283	101.48	292.10	-166.13	-54.05	11.10	11.50	11.11	0.169
250	-342.65	30.5	45	-360	-151.68	0.284	98.67	290.84	-166.40	-53.90	11.03	11.79	11.43	0.177
250	-342.65	30.5	50	-360	-128.53	0.289	95.81	289.80	-166.60	-53.77	10.98	12.03	11.69	0.186
250	-342.65	30.5	40	-380	-194.82	0.295	98.92	289.41	-166.98	-53.74	10.96	11.38	10.99	0.180
250	-342.65	30.5	45	-380	-171.68	0.297	96.10	288.63	-167.08	-53.64	10.92	11.69	11.35	0.189
250	-342.65	31.0	65	-240	60.91	0.298	102.71	270.76	-174.70	-51.72	9.96	12.85	12.41	0.150
250	-342.65	31.0	55	-260	-5.38	0.300	105.09	268.73	-175.74	-51.52	9.85	12.54	12.13	0.145
250	-342.65	31.0	60	-260	17.77	0.289	102.12	264.87	-177.05	-51.08	9.65	12.68	12.27	0.153
250	-342.65	31.0	65	-260	40.91	0.292	98.72	258.56	-179.30	-50.37	9.32	12.80	12.38	0.161
250	-342.65	31.0	70	-260	64.06	0.296	94.45	246.14	-183.96	-48.99	8.66	12.92	12.49	0.171
250	-342.65	31.0	50	-280	-48.53	0.298	104.41	259.61	-179.33	-50.52	9.37	12.32	11.93	0.149
250	-342.65	31.0	55	-280	-25.38	0.286	100.39	247.96	-183.68	-49.22	8.75	12.48	12.09	0.158
250	-342.65	31.0	60	-280	-2.23	0.282	93.42	215.04	-196.45	-45.59	7.01	12.63	12.22	0.171
250	-342.65	31.0	70	-280	44.06	0.296	106.69	362.06	-139.21	-61.79	14.80	12.88	12.44	0.164
250	-342.65	31.0	55	-300	-45.38	0.273	113.41	370.56	-136.58	-62.78	15.24	12.42	12.04	0.150
250	-342.65	31.0	60	-300	-22.23	0.279	105.19	322.66	-154.42	-57.44	12.71	12.58	12.18	0.164
250	-342.65	31.0	65	-300	0.91	0.283	100.71	308.43	-159.67	-55.85	11.96	12.71	12.30	0.174
250	-342.65	31.0	70	-300	24.06	0.291	97.06	301.51	-162.14	-55.07	11.60	12.84	12.41	0.184
250	-342.65	31.0	40	-320	-134.82	0.277	120.24	380.32	-133.16	-63.89	15.75	11.72	11.26	0.137
250	-342.65	31.0	45	-320	-111.68	0.279	111.15	325.02	-153.96	-57.73	12.83	11.97	11.56	0.151
250	-342.65	31.0	50	-320	-88.53	0.277	106.71	309.69	-159.64	-56.02	12.02	12.18	11.80	0.161
250	-342.65	31.0	55	-320	-65.38	0.279	103.17	302.38	-162.23	-55.20	11.64	12.36	11.98	0.170
250	-342.65	31.0	60	-320	-42.23	0.282	99.92	298.07	-163.68	-54.70	11.41	12.52	12.13	0.178
250	-342.65	31.0	65	-320	-19.09	0.287	96.77	295.17	-164.58	-54.37	11.26	12.67	12.27	0.187
250	-342.65	31.0	70	-320	4.06	0.297	93.62	293.07	-165.18	-54.12	11.16	12.80	12.37	0.196
250	-342.65	31.0	40	-340	-154.82	0.285	108.98	303.34	-162.34	-55.34	11.68	11.61	11.16	0.157
250	-342.65	31.0	45	-340	-131.68	0.280	105.79	298.80	-163.83	-54.82	11.45	11.88	11.49	0.165

250	-342.65	31.0	50	-340	-108.53	0.280	102.79	295.82	-164.77	-54.47	11.29	12.11	11.74	0.173
250	-342.65	31.0	55	-340	-85.38	0.282	99.83	293.67	-165.39	-54.22	11.18	12.30	11.92	0.181
250	-342.65	31.0	60	-340	-62.23	0.284	96.85	292.03	-165.83	-54.02	11.10	12.47	12.09	0.190
250	-342.65	31.0	65	-340	-39.09	0.292	93.83	290.72	-166.12	-53.86	11.03	12.62	12.22	0.199
250	-342.65	31.0	40	-360	-174.82	0.294	105.64	294.26	-165.60	-54.32	11.21	11.49	11.05	0.168
250	-342.65	31.0	45	-360	-151.68	0.289	102.84	292.59	-166.04	-54.12	11.12	11.79	11.40	0.176
250	-342.65	31.0	50	-360	-128.53	0.291	99.99	291.25	-166.35	-53.95	11.05	12.03	11.67	0.184
250	-342.65	31.0	55	-360	-105.38	0.293	97.08	290.15	-166.57	-53.82	11.00	12.23	11.86	0.193
250	-342.65	31.0	60	-360	-82.23	0.298	94.10	289.21	-166.72	-53.70	10.95	12.41	12.04	0.202
250	-342.65	31.5	65	-260	40.91	0.295	103.82	266.44	-176.68	-51.27	9.73	12.81	12.36	0.159
250	-342.65	31.5	70	-260	64.06	0.292	100.32	260.98	-178.47	-50.64	9.44	12.93	12.47	0.168
250	-342.65	31.5	60	-280	-2.23	0.297	102.30	252.67	-181.93	-49.75	9.00	12.64	12.20	0.164
250	-342.65	31.5	65	-280	20.91	0.287	96.78	230.45	-190.46	-47.29	7.83	12.77	12.33	0.175
250	-342.65	31.5	60	-300	-22.23	0.275	120.95	422.60	-117.00	-68.57	17.98	12.58	12.17	0.151
250	-342.65	31.5	65	-300	0.91	0.281	107.46	330.96	-151.36	-58.37	13.15	12.72	12.28	0.170
250	-342.65	31.5	70	-300	24.06	0.284	102.34	311.74	-158.50	-56.22	12.14	12.85	12.40	0.181
250	-342.65	31.5	45	-320	-111.68	0.274	129.58	448.96	-107.61	-71.54	19.36	11.97	11.53	0.136
250	-342.65	31.5	50	-320	-88.53	0.285	113.62	334.21	-150.57	-58.76	13.31	12.19	11.77	0.157
250	-342.65	31.5	55	-320	-65.38	0.282	108.42	313.20	-158.38	-56.42	12.21	12.37	11.96	0.167
250	-342.65	31.5	60	-320	-42.23	0.282	104.67	304.28	-161.61	-55.42	11.74	12.53	12.11	0.176
250	-342.65	31.5	65	-320	-19.09	0.285	101.30	299.27	-163.33	-54.84	11.48	12.67	12.25	0.185
250	-342.65	31.5	70	-320	4.06	0.287	98.05	296.01	-164.36	-54.47	11.31	12.80	12.37	0.194
250	-342.65	31.5	45	-340	-131.68	0.297	110.46	305.26	-161.66	-55.56	11.78	11.88	11.45	0.163
250	-342.65	31.5	50	-340	-108.53	0.289	107.23	300.04	-163.46	-54.96	11.51	12.11	11.70	0.171
250	-342.65	31.5	55	-340	-85.38	0.284	104.19	296.70	-164.55	-54.58	11.34	12.30	11.90	0.180
250	-342.65	31.5	60	-340	-62.23	0.286	101.15	294.32	-165.25	-54.30	11.21	12.47	12.07	0.188
250	-342.65	31.5	65	-340	-39.09	0.289	98.09	292.54	-165.73	-54.09	11.12	12.62	12.20	0.197
250	-342.65	31.5	70	-340	-15.94	0.293	95.00	291.12	-166.05	-53.91	11.05	12.76	12.32	0.206
250	-342.65	31.5	50	-360	-128.53	0.296	104.15	293.11	-165.94	-54.18	11.15	12.03	11.64	0.183
250	-342.65	31.5	55	-360	-105.38	0.298	101.27	291.68	-166.29	-54.01	11.07	12.24	11.84	0.191
250	-342.65	32.0	70	-300	24.06	0.284	110.22	343.49	-146.69	-59.76	13.81	12.85	12.38	0.175
250	-342.65	32.0	55	-320	-65.38	0.290	116.67	348.43	-145.28	-60.35	14.06	12.37	11.95	0.161
250	-342.65	32.0	60	-320	-42.23	0.288	110.29	317.75	-156.77	-56.93	12.45	12.54	12.10	0.173
250	-342.65	32.0	65	-320	-19.09	0.285	106.18	306.51	-160.85	-55.67	11.85	12.68	12.23	0.183
250	-342.65	32.0	70	-320	4.06	0.287	102.65	300.62	-162.90	-55.00	11.55	12.81	12.35	0.192
250	-342.65	32.0	55	-340	-85.38	0.299	108.69	301.47	-163.03	-55.13	11.58	12.31	11.89	0.178
250	-342.65	32.0	60	-340	-62.23	0.292	105.54	297.65	-164.28	-54.69	11.39	12.48	12.06	0.186
250	-342.65	32.0	65	-340	-39.09	0.292	102.42	295.02	-165.07	-54.38	11.25	12.63	12.18	0.195
250	-342.65	32.0	70	-340	-15.94	0.297	99.32	293.07	-165.61	-54.15	11.15	12.76	12.32	0.204
250	-342.65	32.5	60	-320	-42.23	0.295	120.97	373.46	-135.93	-63.14	15.38	12.54	12.08	0.165
250	-342.65	32.5	70	-320	4.06	0.289	107.74	309.24	-159.91	-55.98	12.00	12.82	12.33	0.189
250	-342.65	33.0	65	-320	-19.09	0.295	128.82	429.49	-115.03	-69.38	18.34	12.69	12.20	0.164
255	-327.65	30.0	45	-240	-27.82	0.275	105.28	267.34	-172.94	-51.11	9.83	12.32	12.01	0.120
255	-327.65	30.0	50	-240	-4.24	0.270	102.78	265.44	-173.51	-50.88	9.73	12.48	12.17	0.127

255	-327.65	30.0	65	-240	66.48	0.296	94.20	254.87	-177.08	-49.68	9.18	12.87	12.54	0.150
255	-327.65	30.0	40	-260	-71.40	0.279	105.17	263.03	-174.64	-50.63	9.60	12.06	11.73	0.123
255	-327.65	30.0	45	-260	-47.82	0.267	102.45	259.57	-175.80	-50.24	9.42	12.25	11.94	0.131
255	-327.65	30.0	50	-260	-24.24	0.265	99.48	254.56	-177.58	-49.67	9.16	12.42	12.12	0.138
255	-327.65	30.0	55	-260	-0.67	0.270	96.05	246.53	-180.55	-48.77	8.73	12.57	12.26	0.147
255	-327.65	30.0	60	-260	22.91	0.278	91.56	231.28	-186.36	-47.08	7.93	12.71	12.40	0.157
255	-327.65	30.0	65	-260	46.48	0.287	83.51	190.61	-202.34	-42.61	5.77	12.83	12.50	0.172
255	-327.65	30.0	40	-280	-91.40	0.274	101.08	245.65	-181.28	-48.71	8.68	11.98	11.64	0.135
255	-327.65	30.0	45	-280	-67.82	0.271	96.54	228.98	-187.65	-46.86	7.80	12.18	11.88	0.145
255	-327.65	30.0	50	-280	-44.24	0.278	87.59	181.50	-206.37	-41.65	5.28	12.36	12.06	0.161
255	-327.65	30.0	60	-280	2.91	0.282	109.39	392.75	-124.20	-64.93	16.47	12.66	12.35	0.143
255	-327.65	30.0	65	-280	26.48	0.296	99.78	333.47	-146.45	-58.34	13.34	12.79	12.47	0.159
255	-327.65	30.0	45	-300	-87.82	0.264	113.52	380.91	-129.06	-63.65	15.84	12.11	11.80	0.133
255	-327.65	30.0	50	-300	-64.24	0.271	105.11	330.94	-147.82	-58.09	13.20	12.30	12.00	0.147
255	-327.65	30.0	55	-300	-40.67	0.278	100.45	313.74	-154.20	-56.17	12.30	12.46	12.17	0.157
255	-327.65	30.0	60	-300	-17.09	0.290	96.77	304.97	-157.37	-55.18	11.84	12.61	12.30	0.166
255	-327.65	30.0	40	-320	-131.40	0.266	105.81	312.97	-154.90	-56.11	12.25	11.80	11.46	0.144
255	-327.65	30.0	45	-320	-107.82	0.268	102.32	304.71	-157.87	-55.18	11.82	12.03	11.73	0.153
255	-327.65	30.0	50	-320	-84.24	0.275	99.14	299.59	-159.65	-54.60	11.55	12.23	11.94	0.161
255	-327.65	30.0	55	-320	-60.67	0.286	96.12	296.08	-160.82	-54.20	11.37	12.41	12.12	0.170
255	-327.65	30.0	40	-340	-151.40	0.274	101.67	296.20	-161.17	-54.24	11.37	11.70	11.37	0.157
255	-327.65	30.0	45	-340	-127.82	0.276	98.84	293.68	-161.95	-53.95	11.24	11.95	11.66	0.165
255	-327.65	30.0	50	-340	-104.24	0.288	96.00	291.73	-162.51	-53.72	11.14	12.16	11.88	0.173
255	-327.65	30.0	40	-360	-171.40	0.293	98.82	290.44	-163.22	-53.59	11.06	11.59	11.27	0.168
255	-327.65	30.5	50	-240	-4.24	0.288	106.86	268.06	-172.80	-51.20	9.87	12.49	12.16	0.127
255	-327.65	30.5	55	-240	19.33	0.276	104.34	266.30	-173.29	-50.99	9.78	12.63	12.30	0.133
255	-327.65	30.5	60	-240	42.91	0.275	101.68	264.09	-173.98	-50.73	9.66	12.76	12.42	0.141
255	-327.65	30.5	65	-240	66.48	0.280	98.86	261.15	-174.92	-50.39	9.51	12.88	12.53	0.148
255	-327.65	30.5	70	-240	90.06	0.289	95.84	257.06	-176.34	-49.93	9.29	12.99	12.63	0.157
255	-327.65	30.5	45	-260	-47.82	0.293	106.81	264.19	-174.32	-50.77	9.66	12.26	11.93	0.130
255	-327.65	30.5	50	-260	-24.24	0.278	104.12	261.15	-175.32	-50.42	9.50	12.43	12.10	0.137
255	-327.65	30.5	55	-260	-0.67	0.269	101.21	256.87	-176.80	-49.94	9.28	12.58	12.25	0.144
255	-327.65	30.5	60	-260	22.91	0.270	97.92	250.31	-179.18	-49.20	8.93	12.72	12.38	0.153
255	-327.65	30.5	65	-260	46.48	0.272	93.91	238.81	-183.50	-47.92	8.33	12.84	12.50	0.162
255	-327.65	30.5	70	-260	70.06	0.280	87.88	213.07	-193.47	-45.08	6.96	12.96	12.59	0.175
255	-327.65	30.5	45	-280	-67.82	0.286	103.05	249.71	-179.81	-49.16	8.90	12.19	11.85	0.141
255	-327.65	30.5	50	-280	-44.24	0.278	99.07	237.30	-184.49	-47.78	8.24	12.37	12.04	0.150
255	-327.65	30.5	55	-280	-20.67	0.278	92.72	208.28	-195.77	-44.58	6.70	12.53	12.21	0.162
255	-327.65	30.5	70	-280	50.06	0.285	102.81	347.95	-141.04	-59.95	14.11	12.92	12.56	0.164
255	-327.65	30.5	50	-300	-64.24	0.263	122.28	445.09	-105.14	-70.80	19.22	12.30	11.98	0.132
255	-327.65	30.5	55	-300	-40.67	0.270	108.03	343.71	-143.07	-59.51	13.88	12.47	12.16	0.152
255	-327.65	30.5	60	-300	-17.09	0.274	102.45	319.13	-152.25	-56.77	12.58	12.62	12.30	0.163
255	-327.65	30.5	65	-300	6.48	0.281	98.44	307.96	-156.34	-55.52	11.99	12.75	12.42	0.172
255	-327.65	30.5	70	-300	30.06	0.294	94.91	301.52	-158.61	-54.79	11.66	12.88	12.51	0.182

255 -327.65 30.5 40 -320 -131.40	0.266	112.96 340.06 -144.86 -59.14 13.68 11.80 11.43 0.140
255 -327.65 30.5 50 -320 -84.24	0.271	104.05 307.55 -156.91 -55.51 11.96 12.24 11.92 0.159
255 -327.65 30.5 55 -320 -60.67	0.272	100.73 301.44 -159.06 -54.82 11.64 12.41 12.10 0.168
255 -327.65 30.5 60 -320 -37.09	0.277	97.58 297.38 -160.42 -54.35 11.43 12.57 12.25 0.177
255 -327.65 30.5 65 -320 -13.52	0.291	94.49 294.46 -161.35 -54.01 11.28 12.71 12.37 0.185
255 -327.65 30.5 40 -340 -151.40	0.282	106.16 301.36 -159.49 -54.84 11.63 11.69 11.33 0.155
255 -327.65 30.5 45 -340 -127.82	0.284	103.20 297.46 -160.79 -54.39 11.43 11.95 11.63 0.164
255 -327.65 30.5 50 -340 -104.24	0.287	100.28 294.63 -161.68 -54.06 11.28 12.17 11.86 0.172
255 -327.65 30.5 55 -340 -80.67	0.290	97.39 292.49 -162.32 -53.81 11.17 12.35 12.04 0.180
255 -327.65 31.0 60 -240 42.91	0.288	105.87 267.11 -173.11 -51.09 9.82 12.77 12.42 0.140
255 -327.65 31.0 65 -240 66.48	0.278	103.21 265.09 -173.70 -50.85 9.71 12.89 12.51 0.147
255 -327.65 31.0 70 -240 90.06	0.281	100.39 262.48 -174.53 -50.55 9.58 13.00 12.61 0.155
255 -327.65 31.0 55 -260 -0.67	0.291	105.74 262.54 -174.91 -50.59 9.57 12.59 12.23 0.143
255 -327.65 31.0 60 -260 22.91	0.277	102.87 258.84 -176.17 -50.16 9.38 12.72 12.37 0.151
255 -327.65 31.0 65 -260 46.48	0.272	99.67 253.36 -178.10 -49.54 9.09 12.85 12.48 0.159
255 -327.65 31.0 70 -260 70.06	0.275	95.96 244.37 -181.43 -48.54 8.62 12.96 12.59 0.168
255 -327.65 31.0 50 -280 -44.24	0.299	104.93 252.97 -178.67 -49.53 9.07 12.37 12.03 0.147
255 -327.65 31.0 55 -280 -20.67	0.286	101.27 243.34 -182.24 -48.46 8.56 12.53 12.19 0.156
255 -327.65 31.0 60 -280 2.91	0.282	96.18 223.65 -189.80 -46.28 7.52 12.68 12.32 0.166
255 -327.65 31.0 65 -280 26.48	0.294	84.57 159.25 -215.43 -39.23 4.10 12.81 12.43 0.186
255 -327.65 31.0 60 -300 -17.09	0.271	111.90 364.71 -135.22 -61.85 14.98 12.63 12.28 0.155
255 -327.65 31.0 65 -300 6.48	0.274	104.61 326.40 -149.58 -57.59 12.96 12.76 12.40 0.168
255 -327.65 31.0 70 -300 30.06	0.277	100.17 311.64 -155.02 -55.94 12.19 12.88 12.51 0.179
255 -327.65 31.0 45 -320 -107.82	0.274	116.57 358.11 -138.14 -61.15 14.63 12.04 11.68 0.144
255 -327.65 31.0 50 -320 -84.24	0.274	110.03 324.63 -150.67 -57.42 12.86 12.24 11.91 0.156
255 -327.65 31.0 55 -320 -60.67	0.277	105.84 311.03 -155.68 -55.90 12.15 12.42 12.08 0.165
255 -327.65 31.0 60 -320 -37.09	0.280	102.30 303.59 -158.34 -55.06 11.76 12.57 12.23 0.174
255 -327.65 31.0 65 -320 -13.52	0.284	99.04 298.86 -159.96 -54.52 11.51 12.72 12.37 0.183
255 -327.65 31.0 70 -320 10.06	0.290	95.85 295.53 -161.02 -54.14 11.34 12.84 12.47 0.192
255 -327.65 31.0 45 -340 -127.82	0.297	107.83 303.43 -158.81 -55.08 11.74 11.95 11.61 0.162
255 -327.65 31.0 50 -340 -104.24	0.295	104.75 298.91 -160.36 -54.56 11.51 12.17 11.84 0.170
255 -327.65 31.0 55 -340 -80.67	0.297	101.75 295.71 -161.39 -54.19 11.34 12.36 12.02 0.178
255 -327.65 31.5 65 -240 66.48	0.300	107.38 267.84 -172.95 -51.18 9.85 12.90 12.51 0.146
255 -327.65 31.5 70 -240 90.06	0.286	104.70 266.00 -173.47 -50.96 9.76 13.01 12.59 0.154
255 -327.65 31.5 60 -260 46.48	0.288	104.45 260.52 -175.63 -50.36 9.47 12.86 12.46 0.157
255 -327.65 31.5 70 -260 70.06	0.279	101.36 255.88 -177.24 -49.83 9.23 12.97 12.57 0.165
255 -327.65 31.5 60 -280 2.91	0.297	103.25 247.92 -180.56 -48.97 8.80 12.68 12.32 0.162
255 -327.65 31.5 65 -280 26.48	0.288	98.85 233.62 -185.97 -47.38 8.05 12.81 12.43 0.171
255 -327.65 31.5 70 -280 50.06	0.291	91.30 197.21 -200.22 -43.37 6.12 12.93 12.52 0.185
255 -327.65 31.5 65 -300 6.48	0.274	118.05 405.81 -119.86 -66.43 17.15 12.77 12.39 0.157
255 -327.65 31.5 70 -300 30.06	0.279	107.24 336.80 -145.72 -58.75 13.51 12.89 12.50 0.173
255 -327.65 31.5 50 -320 -84.24	0.285	121.94 391.37 -125.72 -64.86 16.38 12.25 11.89 0.147
255 -327.65 31.5 55 -320 -60.67	0.287	112.57 334.00 -147.22 -58.47 13.36 12.43 12.07 0.161
255 -327.65 31.5 60 -320 -37.09	0.288	107.71 315.43 -154.11 -56.40 12.38 12.58 12.21 0.171

255	-327.65	31.5	65	-320	-13.52	0.291	103.93	306.17	-157.46	-55.36	11.89	12.72	12.35	0.181
255	-327.65	31.5	70	-320	10.06	0.295	100.49	300.55	-159.40	-54.72	11.60	12.85	12.47	0.190
255	-327.65	32.0	70	-280	50.06	0.297	101.12	240.67	-183.34	-48.17	8.42	12.94	12.52	0.177
255	-327.65	32.0	70	-300	30.06	0.279	132.41	523.18	-76.42	-79.54	23.33	12.90	12.48	0.149
255	-327.65	32.0	55	-320	-60.67	0.290	132.68	473.38	-95.25	-74.01	20.70	12.43	12.05	0.144
255	-327.65	32.0	65	-320	-13.52	0.298	109.73	321.19	-152.03	-57.04	12.68	12.73	12.34	0.177
260	-312.65	30.0	40	-240	-48.10	0.293	108.14	263.41	-171.42	-50.43	9.67	12.19	11.91	0.112
260	-312.65	30.0	45	-240	-24.11	0.278	105.82	261.81	-171.88	-50.25	9.59	12.37	12.10	0.119
260	-312.65	30.0	50	-240	-0.12	0.268	103.39	259.86	-172.47	-50.02	9.49	12.52	12.27	0.125
260	-312.65	30.0	55	-240	23.86	0.266	100.80	257.44	-173.24	-49.74	9.36	12.67	12.40	0.132
260	-312.65	30.0	60	-240	47.85	0.266	98.08	254.31	-174.28	-49.38	9.20	12.80	12.53	0.140
260	-312.65	30.0	65	-240	71.84	0.272	95.14	250.08	-175.75	-48.90	8.98	12.91	12.63	0.148
260	-312.65	30.0	70	-240	95.83	0.279	91.89	244.02	-177.94	-48.22	8.66	13.02	12.73	0.156
260	-312.65	30.0	40	-260	-68.10	0.284	105.57	256.90	-173.81	-49.71	9.33	12.11	11.83	0.122
260	-312.65	30.0	45	-260	-44.11	0.273	102.96	253.47	-174.98	-49.31	9.15	12.30	12.04	0.129
260	-312.65	30.0	50	-260	-20.12	0.267	100.11	248.77	-176.65	-48.78	8.90	12.47	12.22	0.137
260	-312.65	30.0	55	-260	3.86	0.268	96.87	241.81	-179.19	-48.00	8.54	12.62	12.36	0.145
260	-312.65	30.0	60	-260	27.85	0.270	92.99	230.47	-183.47	-46.74	7.94	12.75	12.48	0.154
260	-312.65	30.0	65	-260	51.84	0.278	87.57	208.38	-192.02	-44.30	6.77	12.87	12.60	0.165
260	-312.65	30.0	40	-280	-88.10	0.282	101.44	239.14	-180.61	-47.74	8.39	12.04	11.74	0.134
260	-312.65	30.0	45	-280	-64.11	0.279	97.39	225.37	-185.86	-46.21	7.66	12.24	11.98	0.143
260	-312.65	30.0	50	-280	-40.12	0.284	91.05	196.05	-197.31	-42.98	6.11	12.41	12.16	0.156
260	-312.65	30.0	70	-280	55.83	0.296	99.39	337.98	-141.36	-58.57	13.63	12.94	12.66	0.163
260	-312.65	30.0	50	-300	-60.12	0.265	110.72	365.54	-131.48	-61.68	15.08	12.35	12.10	0.139
260	-312.65	30.0	55	-300	-36.14	0.272	104.07	330.54	-144.59	-57.78	13.23	12.51	12.26	0.151
260	-312.65	30.0	60	-300	-12.15	0.282	99.66	315.03	-150.33	-56.04	12.42	12.66	12.40	0.161
260	-312.65	30.0	65	-300	11.84	0.297	95.98	306.23	-153.52	-55.06	11.96	12.79	12.52	0.171
260	-312.65	30.0	40	-320	-128.10	0.280	108.59	324.84	-147.14	-57.18	12.93	11.87	11.58	0.140
260	-312.65	30.0	45	-320	-104.11	0.282	104.68	312.20	-151.81	-55.76	12.26	12.09	11.84	0.149
260	-312.65	30.0	50	-320	-80.12	0.285	101.30	304.63	-154.53	-54.91	11.87	12.29	12.04	0.158
260	-312.65	30.0	55	-320	-56.14	0.292	98.14	299.56	-156.28	-54.34	11.60	12.46	12.22	0.166
260	-312.65	30.5	50	-240	-0.12	0.293	107.48	262.70	-171.68	-50.35	9.63	12.53	12.26	0.125
260	-312.65	30.5	55	-240	23.86	0.277	105.03	260.93	-172.19	-50.15	9.54	12.67	12.40	0.132
260	-312.65	30.5	60	-240	47.85	0.270	102.45	258.75	-172.85	-49.89	9.43	12.80	12.51	0.139
260	-312.65	30.5	65	-240	71.84	0.270	99.76	256.00	-173.74	-49.57	9.29	12.92	12.62	0.146
260	-312.65	30.5	70	-240	95.83	0.271	96.85	252.38	-174.97	-49.16	9.10	13.03	12.71	0.154
260	-312.65	30.5	45	-260	-44.11	0.298	107.32	258.35	-173.39	-49.88	9.40	12.31	12.03	0.128
260	-312.65	30.5	50	-260	-20.12	0.283	104.70	255.34	-174.38	-49.53	9.24	12.48	12.20	0.135
260	-312.65	30.5	55	-260	3.86	0.275	101.91	251.34	-175.76	-49.08	9.04	12.63	12.35	0.143
260	-312.65	30.5	60	-260	27.85	0.272	98.83	245.67	-177.80	-48.44	8.74	12.76	12.47	0.151
260	-312.65	30.5	65	-260	51.84	0.274	95.26	236.92	-181.06	-47.46	8.28	12.88	12.58	0.159
260	-312.65	30.5	70	-260	75.83	0.278	90.71	221.50	-186.93	-45.75	7.46	12.99	12.68	0.170
260	-312.65	30.5	45	-280	-64.11	0.298	103.56	243.64	-178.97	-48.24	8.62	12.24	11.95	0.140
260	-312.65	30.5	50	-280	-40.12	0.291	99.90	233.29	-182.85	-47.09	8.08	12.42	12.14	0.148

260	-312.65	30.5	55	-280	-16.14	0.290	94.97	213.89	-190.34	-44.95	7.05	12.57	12.29	0.159
260	-312.65	30.5	55	-300	-36.14	0.273	117.02	407.16	-115.94	-66.32	17.27	12.52	12.24	0.140
260	-312.65	30.5	60	-300	-12.15	0.278	107.10	343.78	-139.68	-59.26	13.93	12.66	12.38	0.156
260	-312.65	30.5	65	-300	11.84	0.282	101.81	321.52	-147.96	-56.77	12.76	12.80	12.50	0.167
260	-312.65	30.5	70	-300	35.83	0.292	97.78	310.09	-152.14	-55.49	12.16	12.91	12.61	0.177
260	-312.65	30.5	40	-320	-128.10	0.288	118.72	377.17	-127.61	-63.01	15.69	11.87	11.55	0.133
260	-312.65	30.5	45	-320	-104.11	0.290	111.35	335.07	-143.40	-58.32	13.47	12.10	11.82	0.146
260	-312.65	30.5	50	-320	-80.12	0.293	106.79	317.61	-149.86	-56.37	12.55	12.29	12.02	0.155
260	-312.65	30.5	55	-320	-56.14	0.296	103.11	307.99	-153.35	-55.29	12.04	12.46	12.20	0.164
260	-312.65	30.5	60	-320	-32.15	0.299	99.81	301.87	-155.51	-54.60	11.72	12.61	12.33	0.173
260	-312.65	31.0	60	-240	47.85	0.291	106.64	261.89	-171.95	-50.26	9.59	12.81	12.50	0.138
260	-312.65	31.0	65	-240	71.84	0.279	104.07	259.92	-172.52	-50.03	9.49	12.93	12.61	0.145
260	-312.65	31.0	70	-240	95.83	0.273	101.36	257.48	-173.28	-49.75	9.36	13.04	12.69	0.152
260	-312.65	31.0	60	-260	27.85	0.288	103.65	253.52	-175.03	-49.33	9.15	12.77	12.47	0.149
260	-312.65	31.0	65	-260	51.84	0.282	100.64	248.78	-176.70	-48.79	8.90	12.89	12.58	0.156
260	-312.65	31.0	70	-260	75.83	0.282	97.28	241.80	-179.24	-48.01	8.53	13.00	12.67	0.165
260	-312.65	31.0	60	-280	7.85	0.300	97.92	225.30	-185.94	-46.21	7.66	12.72	12.42	0.163
260	-312.65	31.0	60	-300	-12.15	0.285	131.04	520.76	-73.89	-79.00	23.26	12.67	12.37	0.134
260	-312.65	31.0	65	-300	11.84	0.285	111.27	365.52	-131.73	-61.69	15.08	12.81	12.50	0.159
260	-312.65	31.0	70	-300	35.83	0.293	104.26	330.45	-144.66	-57.77	13.23	12.93	12.60	0.172
260	-312.65	31.0	45	-320	-104.11	0.297	126.66	432.79	-106.89	-69.21	18.62	12.10	11.79	0.133
260	-312.65	31.5	70	-240	95.83	0.292	105.62	260.98	-172.24	-50.16	9.54	13.05	12.69	0.151
260	-312.65	31.5	70	-260	75.83	0.295	102.35	251.37	-175.81	-49.08	9.04	13.01	12.65	0.162
260	-312.65	31.5	70	-300	35.83	0.298	117.23	406.47	-116.24	-66.24	17.24	12.93	12.60	0.160